Composite laminate with embedded electric cables submitted to low energy impact

T. VOGEL[a], J.C. WALRICK[b] , P. CASARI[c]

a. Mechanical Systems Design & Integration
Airbus Group Innovations
12 rue Pasteur, BP76, 92152 Suresnes Cedex, France

b. ESTACA'LAB
ESTACA Campus Ouest
Parc Universitaire Laval-Changé, rueGeorges Charpak, BP76121, Laval Cedex 9, France
jean-christophe.walrick@estaca.fr

c. Institut de Recherche en Génie Civil et Mécanique, UMR CNRS 6183
Université de Nantes
58 rue Michel Ange, BP420, 44606 Saint-Nazaire Cedex, France
Pascal.casari@univ-nantes.fr

Résumé :

Cette étude traite de la résistance mécanique des structures composites fonctionnelles intégrant des systèmes électriques, soumise à l'impact basse énergie. Les matériaux, définis pour des applications aéronautiques sont des stratifiés fibres de verre longues intégrant des couches de câbles électriques. Une question importante porte sur l'endommagement induit par l'impact à basse énergie sur ces structures fonctionnelles et l'influence des couches électriques. L'impact induits des endommagements non forcément visibles en surface qui peuvent induire une dégradation dans l'isolation des conducteurs. Des campagnes d'essais expérimentales sont réalisées à l'aide d'une tour de chute en flexion 3 points dynamique et en impact ponctuel hémisphérique sur éprouvettes clampées à basse énergie (entre 10 et 25 Joules). Des modèles par éléments finis intégrant des mécanismes d'endommagement progressifs couplés à des critères en rupture donne une prédiction des effets mécaniques observés.

Abstract :

The work focuses on the mechanical strength of composite structures with embedded electrical functionalities submitted to low energy impact. This material is defined for aeronautical applications as multilayers of Glass fibre composite with flat electrical cables layers embedded. The main question is about the damage involved by the low energy impact, and its influence on the electrical cables layer. The impact leads to failure with no external signs of damage and insulation degradation. Experimental campaigns are carried out on drop tower test in dynamic bending and hemispherical

punctual impact on clamped specimens at low energy (between 10 and 25 Joules). Finite element models with composite progressive damage laws coupled with failure criterion give a prediction of the different mechanisms.

Mots clefs : multifunctional structures, low energy impacts, damage law, cohesive zone, dielectric strength

1 Introduction

In the last decade, research and development related to multifunctional structures have been increasing due to the growing interest of many industries for these structures and their benefits (cost, mass and volume reduction) [1]. Among those integration of wires into composite structures for electrical function embedded (structural batteries, integrated super capacitors,..). is a key technological challenge for aeronautical and aerospace industry.
While enabling the future of electric and hybrid flight, these structures also have the potential to some weight and volume optimisation as well as to reduce lead time for system installations.

This study focuses on a particular type of multifunctional composite laminated structure composed of 2 laminate embedding layers of flat cable (laminate + cable + laminate) as showed in. Fig. 1.

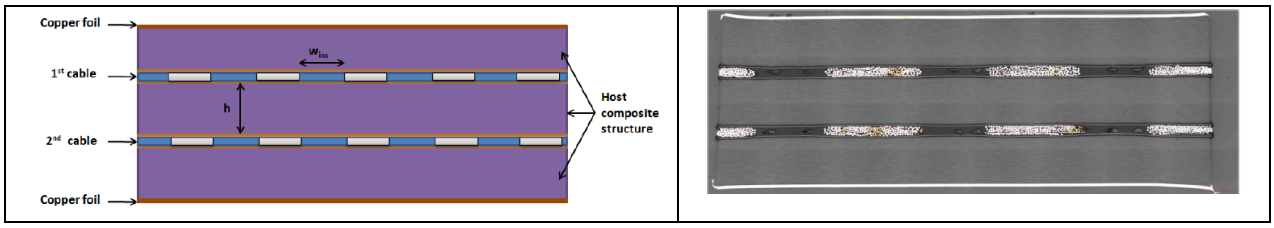

Fig. 1. Representative multifunctional sandwich system with 2 flat cable layers

It is well known that impact loadings can be very harmful to polymeric composite structures as they are likely to produce internal damage such as delamination and fibre/matrix cracking, leading to substantial mechanical properties degradation, including strength and stiffness [3].

To our knowledge very few studies have been carried out to investigate on the impact response of multifunctional structures, and when they do they mainly focus on mechanical properties degradation [4–6]. This study investigate on the mechanical degradation of such structures, but also the influence of a low energy impact on their electrical functionality by insulation deterioration. These considerations are expected to help in determining electrical degradation and acceptance criteria.

The test specimens are composed of 2 layers of flexible flat cable embedded in a host composite structure made of 4 harness-satin equilibrated woven fabric glass-epoxy composite. The flat cables are approximately 0,45mm thick while each composite lay-up is approximately 1,5mm thick, which results in an overall thickness of 5,4mm. The flat cables are inserted in the composite lay-up and the assembly is co-cured in an autoclave for 3 hours at 160°C. The outer stacking sequences of composite plies are $[0/45/0/-45/45/0]_s$ (top and bottom) and the inner stacking sequence is $[-45/0/45/0/-45/0]_s$.
The composite plies, flat electrical cables were manually laid up in this configuration while performing intermediate compacting and suitable surface treatment of the electrical cables (such as dry-cleaning) to ensure good interface properties between the composite and the cables.

In parallel, test specimens without embedded cables (called blank test specimen) are also manufactured to act as references.

2 Three points bending test

The 3 points bend tests are investigated in a first stage for a better understanding of the influence of the integration, through the structure, of flat electrical cables on the damage and critical strength.
This test, in short bending configuration involves inter-laminar shear strains expected critical at the interfaces of the electrical cable layers.

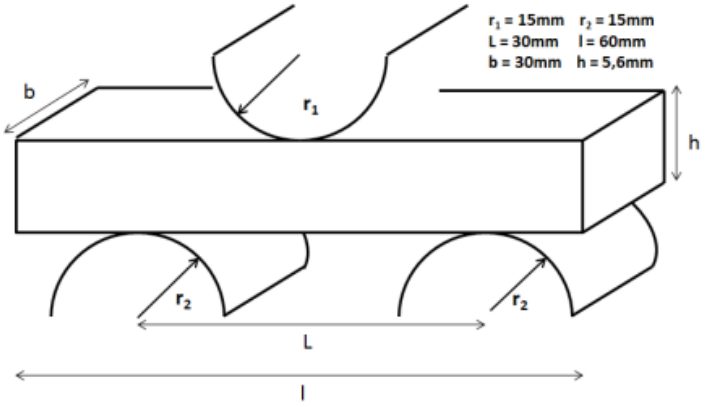

Fig. 2. Configuration of the Short 3 Point Bend Tests

2.1 Quasi-static short 3 points bending tests

Experimental results are compared on test specimens with and without embedded cables. The short 3 points bend tests (S3PB) are carried out according to normative reference ISO 14130. This loading is used for determination of apparent interlaminar shear strength of fibre-plastic composites by the short beam method. Hence, the width of the test specimens is chosen as 5 times the thickness and the length as 10 times the thickness. Besides, the electrical wires were either oriented in the transverse, or longitudinal direction regarding the specimen length to investigate on their influence on the bending stiffness of the structure (Figure. 3)

(a)

(b)

Fig. 3. Two configurations of multifunctional S3PB test specimens: (a) transverse and (b) longitudinal

Test specimens are tested under charge/discharge loading with increments of 1500 N, in order to compare to the results of the S3PB tests on multifunctional test samples compare to same thickness specimen without function embedded (blank specimen test).

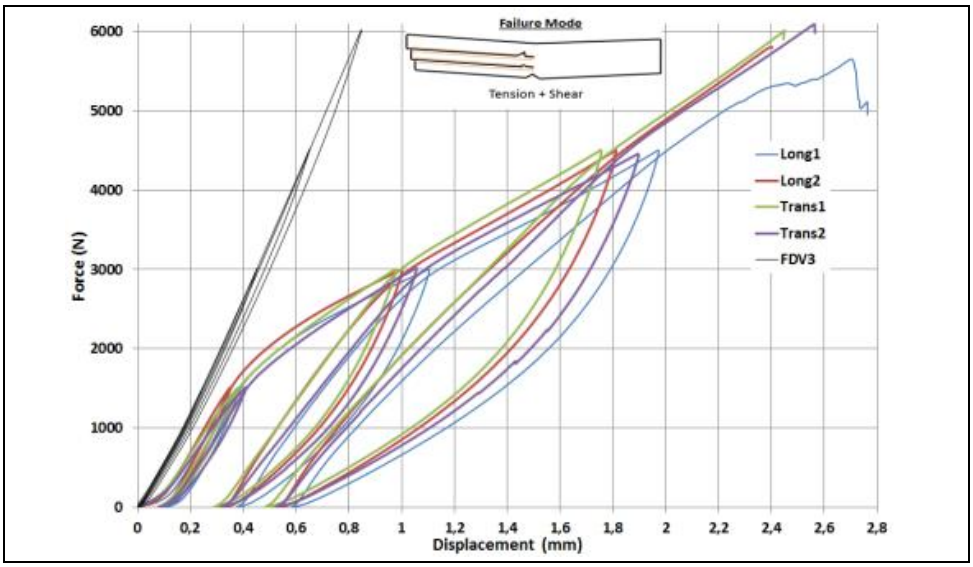

Fig. 4. Short 3 Point Bend for cyclic Test

The first observation that can be drawn is the highly non-linear behaviour of the multifunctional test specimens (transverse and longitudinal) as compared to the blank test specimens (sample ref. FDV3). Indeed, the hysteresis loops are much bigger for multifunctional specimens. Hysteresis loops indicates the presence of energy-dissipative mechanisms, which increase with increasing load.
These energy-dissipative mechanisms are mainly of two natures: firstly probable friction between the test specimen and the test machine supports. Secondly, damage mechanisms within the composite structure (friction between the warp and weft fibres, and fibre/matrix debonding [7]) and for multifunctional specimen, the inter-laminar shear deformation in the embedded cables and the associated damage which could be visually seen during test. These inter-laminar shear strains is revealed through Digital Image Correlations (DIC). In figure 5 where a qualitative measure of the inter-laminar strain field is presented for a displacement of the crosshead of d = 0.5mm. The two electrical cables involves a highly discontinuous load transfer between the three composite layups and a highly non-uniform distribution of the shear stresses through the thickness of the test specimen.

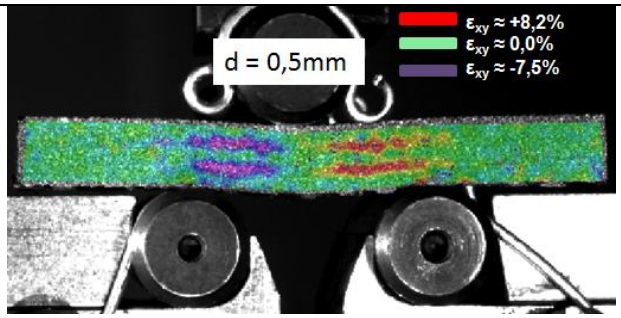

Interlaminar shear strains ε_{xy} observed through DIC on multifunctional S3PB test

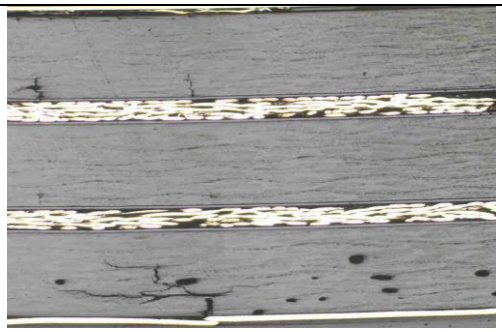

Tensile-shear failure of composite plies in bottom plies and embedded cables interface

Fig. 5. Shear strain and failure distribution through the specimen thickness

It is further noticed that as compared to the reference composite test specimens (FDV1, FDV2), the maximum displacement is significantly increased (by approximately 100%) and the maximum load significantly decreased (by approximately -30%), cf. Table 1.

specimen	**FDV1**	**FDV2**	**Trans 1**	**Trans 2**	**Long 1**	**Long 2**
Maximum Load (N)	8 600	8 900	5 991	5 912	5 360	5 841
Maximum Displacement (mm)	1.20	1.25	2.44	2.36	2.44	2.40

Table 1: Results of the S3PB test on the reference test specimens

The initial bending stiffness of the composite embedding two layers of flat electrical cable varies between 5,000 and 6,000 N/mm which is lower than the bending stiffness of the blank specimens which was measured at 7,700 N/mm.
The second main observation that can be drawn is the non-influence of the orientation of the wires on the mechanical response of the structure. This further confirms the assumption that the out-of-plane deformations are mainly transmitted through the insulator resin of the layer within the cables. Indeed, this is consistent with the observation made in tensile characterisation [6] where through-the-thickness tensile tests had revealed that the weakest interface within the structure was the insulator resin.

2.2 Dynamic short 3 points bending tests

The dynamic bending tests are performed on similar both blank and multifunctional test specimens. The bottom support was kept at 30 mm each other. A specific impact bending test setup was designed, figure 6. The setup was directly mounted on an Imatek IM10-30 drop-weight impact tester with two screwed connectors. The impactor and cylindrical test supports had cylindrical heads of 10 mm diameter, and the impactor total weight was 11,07 kg.

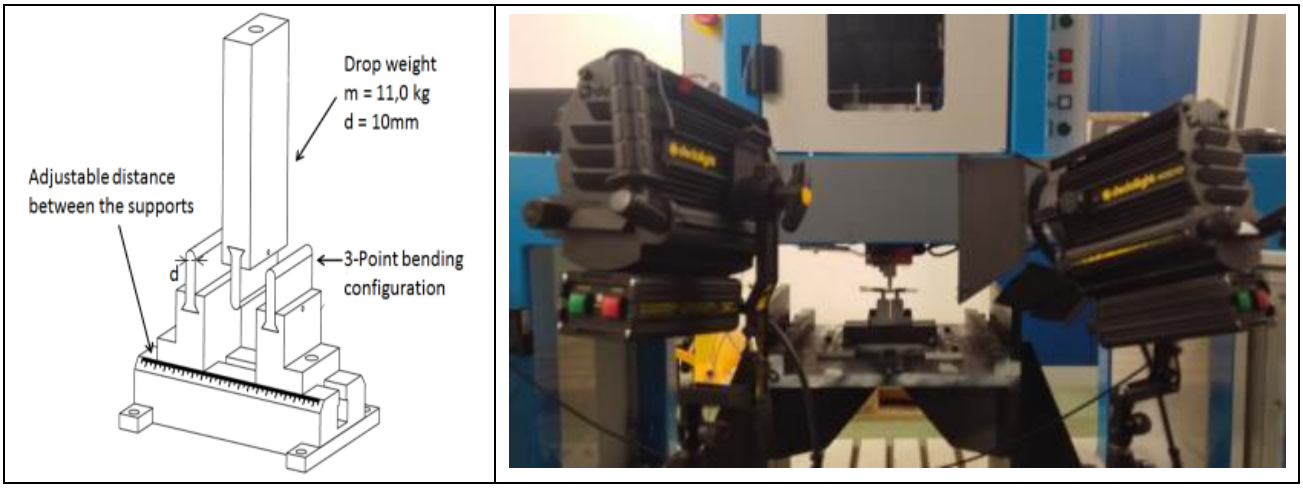

Fig . 6. Impact bending device on the droop test

In the literature, such test setups are not often encountered as impact analysis of composite laminates which are mainly performed on fully clamped specimens during drop weight impact tests [9]–[13]. Yet, some studies deal with the study of the dynamic flexural behaviour of woven composites [8], [14], [15]. Such a configuration is especially expected to provide a better understanding of the influence of boundary conditions on the dynamic response of the structure [16], and to allow performing Digital Image Correlations (DIC).

The impact energies were chosen based on the damage threshold which is considered as the impact energy at which first ply failure occurs on the back face of the test specimens: this resulted in impact tests between 12 Joules and 13 Joules. As the weight of the impactor was kept constant, these energies were achieved by adjusting the height of the impactor. For instance, to obtain an impact energy of 12 Joules with a mass of 11,07kg the droop height of the striker needs to be at 0,11m.
Force – displacement curves for each test are recorded: the displacement is the striker displacement link with the mobile carriage coupled with piezoelectric force sensor (30 KN Kistler dynamic sensor).
The impact events were recorded in 2D via a ultra-high speed camera from the side section of the specimens.

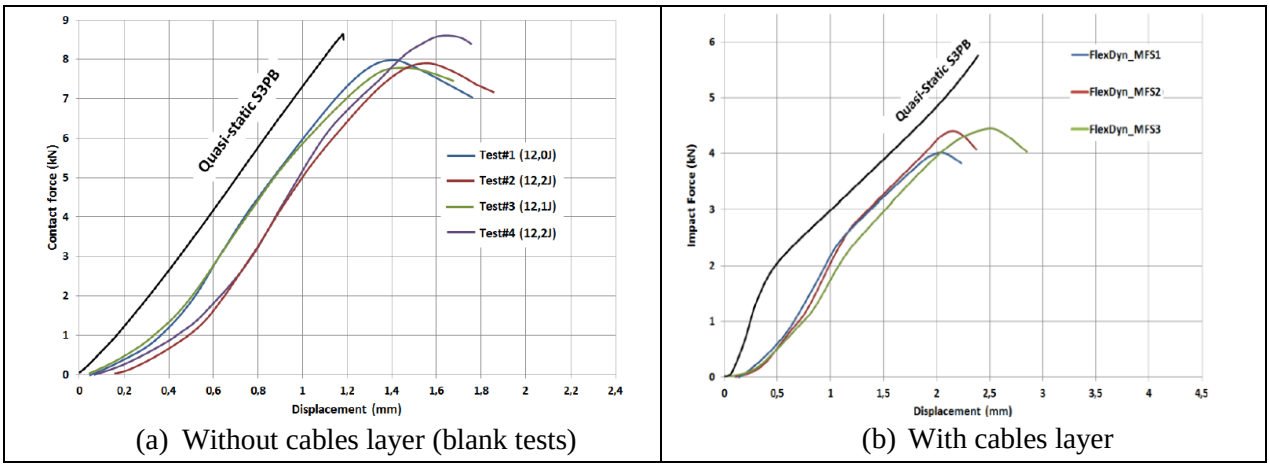

(a) Without cables layer (blank tests) (b) With cables layer

Fig. 7. Contact force-displacement curves for blank test specimen (a) and functional specimen (b)

The force-displacement curves of impact tests are performed on blank tests specimens (a) and multifunctional structure (b) are presented in Figure 7. The effective impact energies were measured between 12 and 13 joules.
For each configuration, test specimens exhibited a similar behaviour as regards to the force-displacement curves. For blank specimens, all test specimens fail at lower peak contact loads (8kN) than the quasi-static test specimens (8,75 kN). The same downward trend is present for the multifunctional specimen like for the quasi-static campaign. For the blank specimens, the main failure mode is a ply failure under tension on the bottom face under bending. For multifunctional test, similarly to the quasi-static measurements, the force-displacement curves can be divided into two parts: the initial loading up to slipping/cohesive damage within the cables, and loading up to ultimate failure. The experimental load-displacement curve seems to be altered due to a non-homogeneous distribution of the load up to 1.0 as sown by DIC analyse.

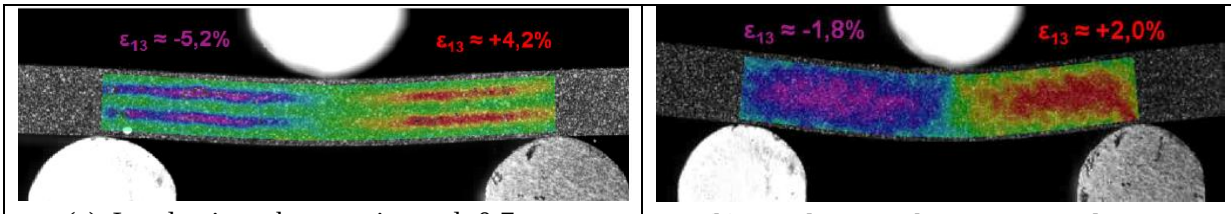

(a) Interlaminar shear strains at d=0.7 mm (b) Interlaminar shear strains at d=2.0 mm

Fig . 8. Digital Image Correlations on (a) multifunctional and (b) blank test specimens

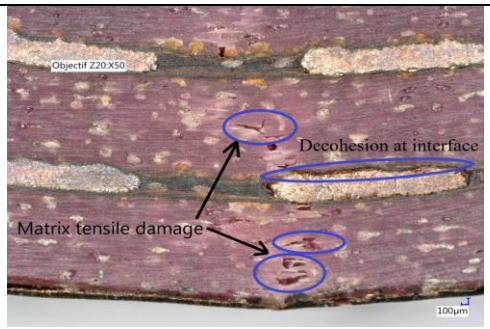

(a) Transverse specimen

(b) Longitudinal specimen

Fig .9. Damage repartition for multifunctional specimen (a) transverse

2.3. Associated numerical progressive model

A model referenced MAT162 coded in LS-DYNA [17] and implemented in ABAQUS via VUMAT is used for correlation with the which is based on the principle of progressive failure of Hashin [18] and damage mechanics of Matzenmiller et al. [19]. The complete model uses a set of seven quadratic failure criteria related to fibre fracture, fibre crush, fibre shear, in-plane matrix crack and delamination. Among these seven failure criteria, only 5 are retained here:

Fibre tension-shear along direction 1

$$f_1 = \left(\frac{E_{11}\langle\varepsilon_{11}\rangle}{X_{1T}}\right)^2 + \left(\frac{G_{13}\varepsilon_{13}}{S_{FS}}\right)^2 - r_1^2 = 0 \quad \text{(Eq.1)}$$

Fibre tension-shear along direction 2

$$f_2 = \left(\frac{E_{22}\langle\varepsilon_{22}\rangle}{X_{2T}}\right)^2 + \left(\frac{G_{23}\varepsilon_{23}}{S_{FS}}\right)^2 - r_2^2 = 0 \quad \text{(Eq.2)}$$

Crush failure under compressive pressure

$$f_5 = \left(\frac{E_{33}\langle-\varepsilon_{33}\rangle}{X_{3C}}\right)^2 - r_5^2 = 0 \quad \text{(Eq.3)}$$

In-plane matrix crack

$$f_6 = \left(\frac{G_{12}\varepsilon_{12}}{S_{12}}\right)^2 - r_6^2 = 0 \quad \text{(Eq.4)}$$

Through-the-thickness matrix crack & delamination

$$f_7 = S_d^2\left[\left(\frac{\langle\sigma_{33}\rangle_+}{Z_T}\right)^2 + \left(\frac{G_{23}\varepsilon_{23}}{S_{23}+S_{SR}}\right)^2 + \left(\frac{G_{13}\varepsilon_{13}}{S_{13}+S_{SR}}\right)^2\right] - r_7^2 = \quad \text{(Eq.5)}$$

With

$$S_{SR} = -\varepsilon_{33}E_{33}\tan\varphi \quad \text{(Eq.6)}$$

S_{SR} stands for the compressive normal strain dependence of the shear strengths (this can be assimilated to the Mohr-Coulomb theory with φ the Coulomb's friction angle).

A positive value of a function f_i denotes the initiation of a specific damage mode with a damage threshold r_i. Damage propagation and post-damage softening behaviour is then controlled by an exponential function associated with a softening parameter m_i (m_1 controls the softening of tensile failure in direction 1, m_2 the softening of tensile failure in direction 2, m_3 the softening related to fibre crush and m_4 the softening due to both in-plane and through-the-thickness matrix cracking). A set of damage variables are then introduced to relate the onset and growth of damage to stiffness losses in the material according to a coupling matrix

that relates a mechanical property to the five modes of damage considered. For instance, damage mode 1 (fibre tension-shear along direction 1) is related to E_1, G_{12} and G_{13} while the delamination criteria is related to E_{33}, G_{13} and G_{23}.

E_{11}	E_{22}	E_{33}	ν_{12}	ν_{13}	ν_{23}	G_{12}	G_{13}	G_{23}
12 GPa	12 GPa	5,6 GPa	0,18	0,40	0,40	2,4 GPa	1,6 GPa	1,6 GPa
X_{1T}	X_{2T}	X_{3C}	S_{12}	S_{23}	S_{13}	S_{FS}	φ	m1
650 MPa	650 MPa	750 MPa	85 MPa	65 MPa	65 MPa	250 MPa	10	0,5
m2	m3	m4						
0,5	1	1						

Table 2. Mechanical properties used to model the glass/epoxy woven fabric

E_{11}	E_{22}	E_{33}	ν_{12}	ν_{13}	ν_{23}	G_{12}	G_{13}	G_{23}
19.5GPa	1.1 GPa	0,48 GPa	0,48	0,48	0,48	0,43 GPa	0,16 GPa	0,16 GPa

Table 3. Mechanical properties of an electrical cable

Experimentally, quasi-static short 3 point bend tests revealed that sliding occurs inside the cables under inter-laminar shear strains. To reproduce this behaviour, cohesive law interactions are defied at the interface between the cables and the composite plies.

The cohesive constitutive law used here is a classical bi-linear mixed-mode traction-separation relationship [20] which is already available within Abaqus CAE, Damage initiation is taken into account with a maximum stress criterion (Eq.7), and damage propagation is modelled with an energy-based Benzeggagh-Kenane (BK) criterion (Eq.8).

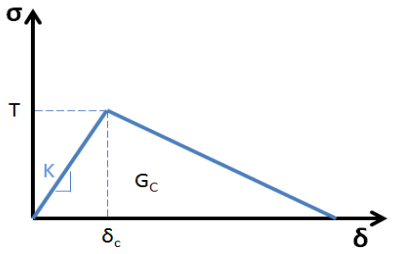

$$max\left\{\frac{\langle\sigma_{33}\rangle}{\overline{T}}, \frac{\sigma_{13}}{S}, \frac{\sigma_{23}}{S}\right\} = 1 \qquad \text{(Eq. 7)}$$

$$G_c = G_{Ic} + (G_{IIc} - G_{Ic})\left(\frac{G_{shear}}{G_T}\right)^{\eta} \qquad \text{(Eq. 8)}$$

Where η is the BK material parameter,

$G_{shear} = G_{II} + G_{III}$, and $G_T = G_I + G_{II} + G_{III}$

The properties used to define the cohesive interactions are listed in Table 1 and have been determined by fitting the experimental results of the Short 3 Point Bend (S3PB) tests with numerical simulations.

T	S	S	G_{Ic}	G_{IIc}	η
14 MPa	20 MPa	20 MPa	0,5 kJ/m²	1 kJ/m²	2

Table 4. Properties used to define the cohesive interactions at interface

2.4. Correlation with experimental bend tests

Numerical models are achieved for short 3 points bend test in an explicit solver with the experimental setup. Solid finite elements are used for composite plies, embedded layers and interfaces between composite plies and embedded layer. Mat 162 as describe previously is associated for composite plies, with cohesive model for interface elements. Numerical results show below correspond to an impact of 13 Joules. Numerical correlations with experimental data help to define the best set of parameters to be used in cohesive zones.

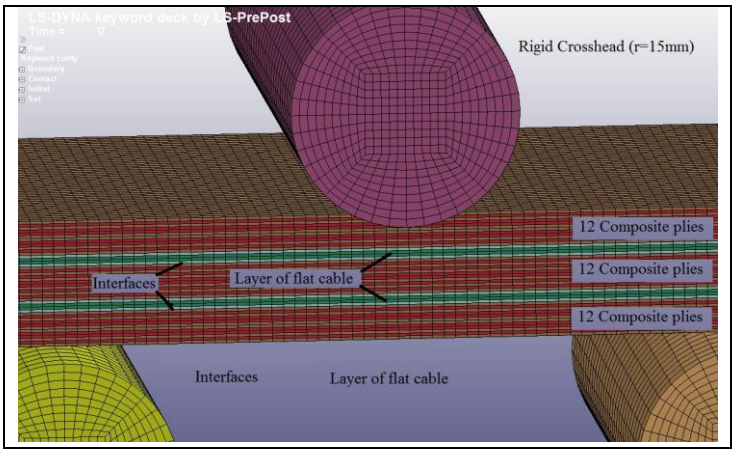

Fig. 10. Bending multifunctional sample model with stacking sequence of solid elements

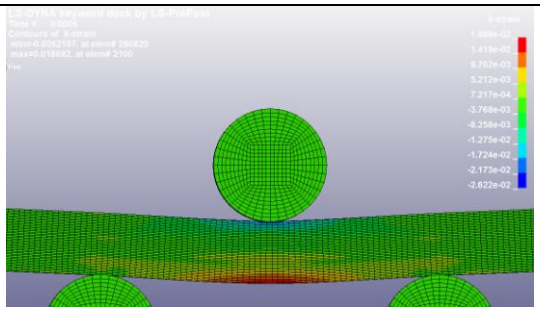

Tensile strains ε_{11} for displacement 0.2 mm

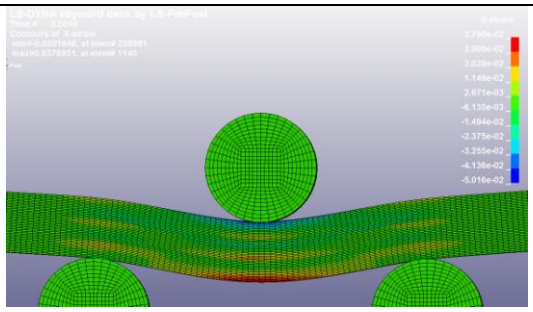

Tensile strains ε_{11} for displacement 0.5 mm

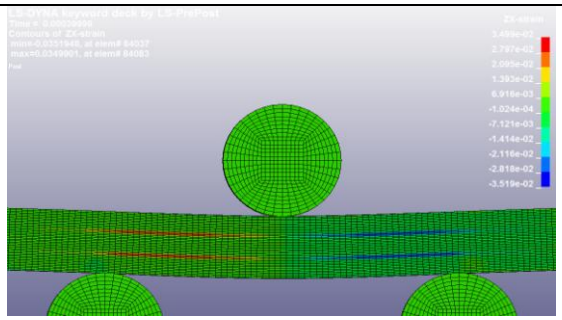

Inter laminar shear strains for 0.2 mm

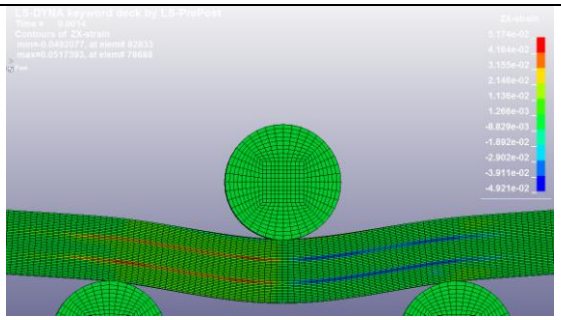

Inter laminar shear strains for 2 mm

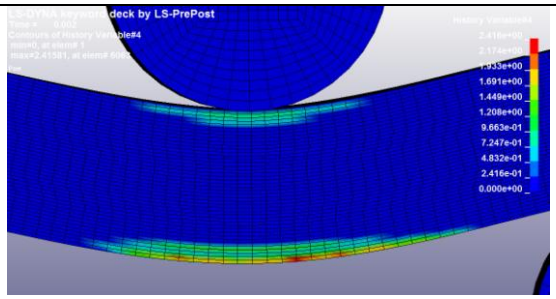

Matrix damage initiation at the sample bottom

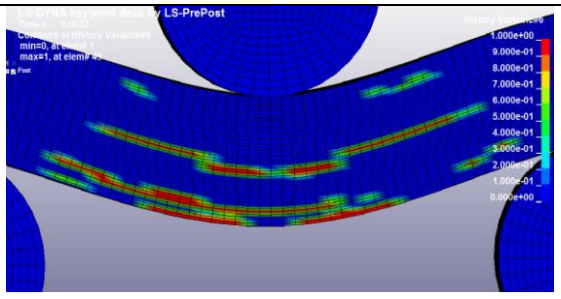

Delamination breakdown between plies

Fig . 11. Numerical strain field and damage results for multifunctional structure model

Under dynamic short 3 point bend test, as well quasi-static, the main strains fields through the sample thickness is mainly in tension at the bottom and inter-laminar shear between plies focused at the embedded cable layer interfaces. The strain gradient lead to local matrix damage initiation and delamination distribution similar to the experimental observations. The level of maximum inter laminar shear strain computed between -3.7% and 5% for displacement close to 2 mm seems similar to the level measured by DIC for experimental tests.
Numerical Force history curves are compared to the experimental for 13 Joules impact bending.
Some fluctuations are present in the dynamic experimental curves due to periodic oscillations along the striker at impact and transmitted to the force sensor. So, this phenomenon is due to the influence of a striker resonant frequency. To prevent loss of information for comparison, the curve is not filtered.
The numerical force follows similar progression regarding experimental behaviour, but seems under-estimate of 10 % the maximal amplitude. Global collapse occurs at the same time, more softly for experimental behaviour.

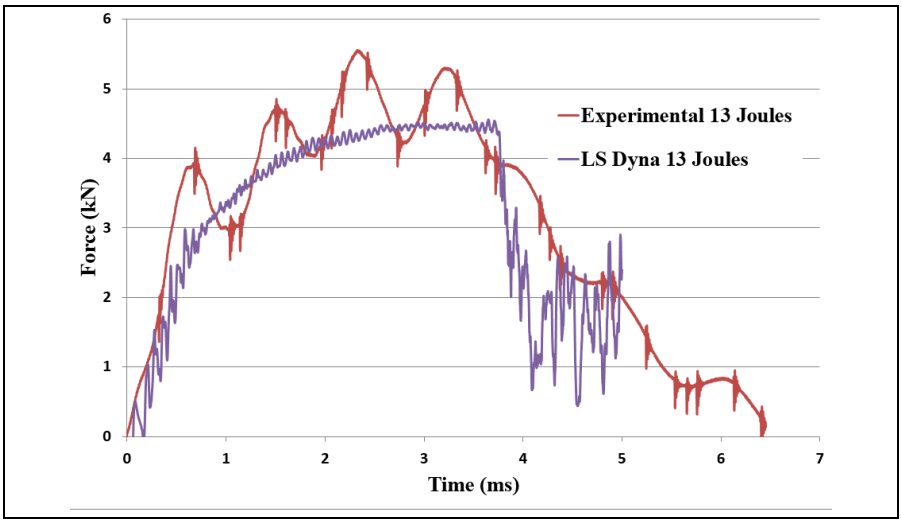

Fig . 12. Contact force history curves comparison

3. Dynamic hemispheric low energy impact test

3.1. Experimental tests and model correlation

Drop weight tests are performed on 60*60 mm^2 test specimens pneumatically clamped to the fixture by means of circular grips between two cylinders with D_{int} = 40 mm and D_{ext} = 60mm (Figure 13). These tests are conducted with a constant impact mass of 9.067Kg at impact energies of 10J, 15J and 20J dropped from a height between 0,11m and 0,22m to reach the impact energies. The hemispherical hardened steel impactor has a diameter of 20mm.

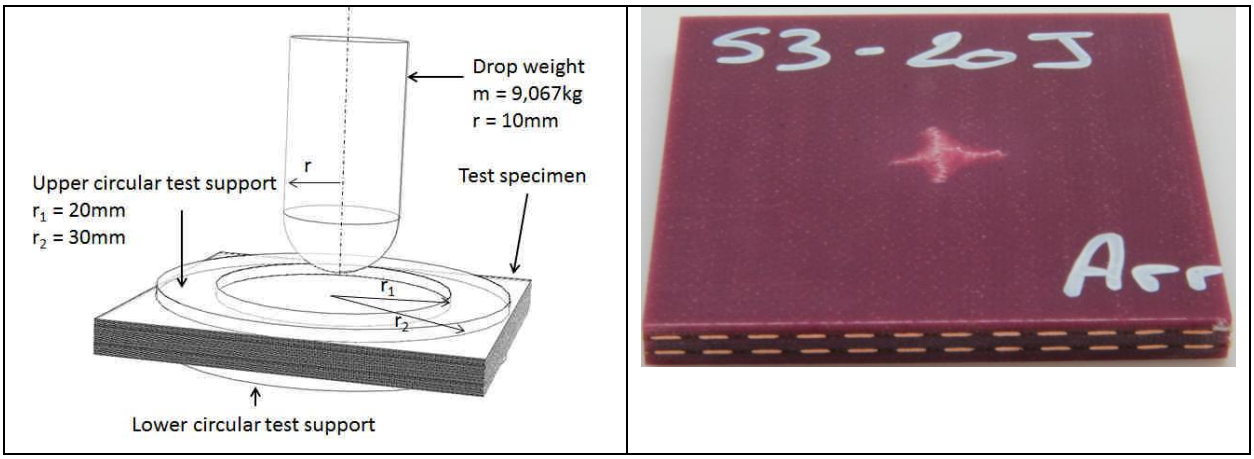

Fig 13. Droop weight impact test setup and impacted specimen with 20 Joules

The contact force history of three test specimens with two layers of embedded cables impacted at 10J, 15J and 20 Joules are plotted in figure 13. As compared to the test specimens without embedded cables, these test specimens show a much more dissipative behaviour with lower peak contact and higher impact durations for the three impact energies.

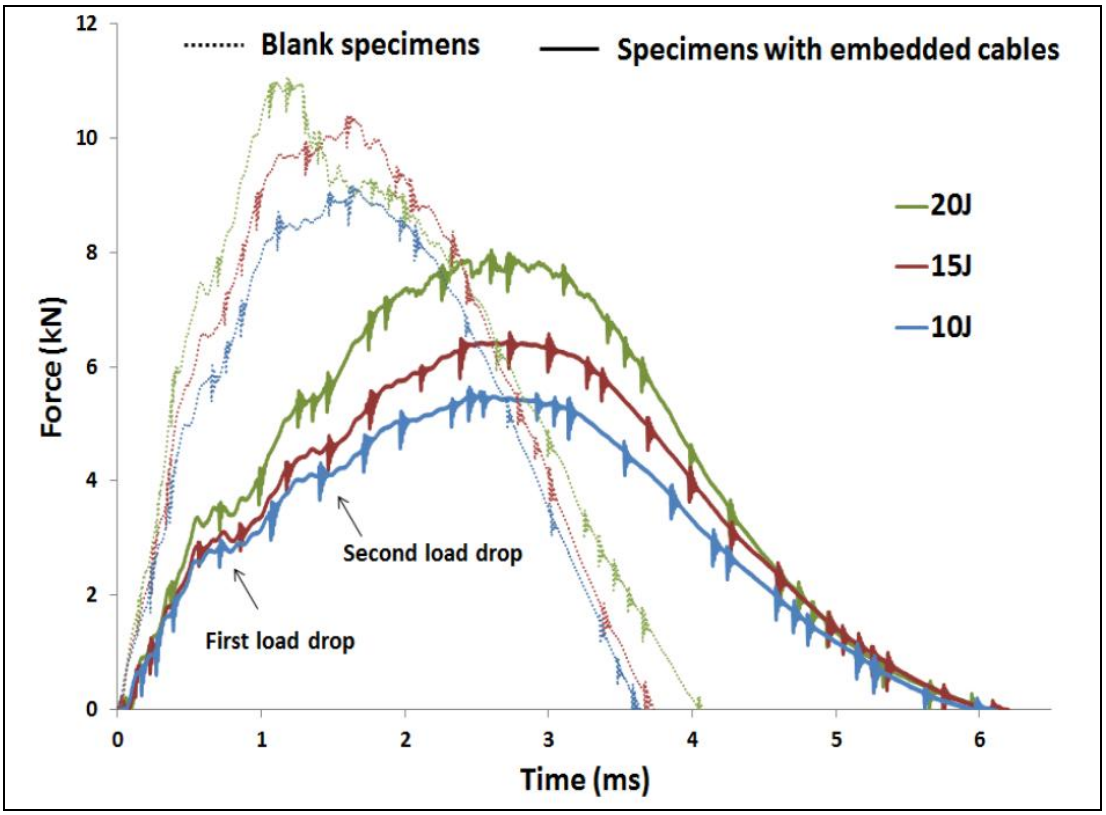

Fig . 14. Contact force histories of multifunctional and blank test specimens

In particular, the multifunctional test specimens seem to exhibit a tri-linear behaviour, with two noticeable load drops. This tri-linear behaviour is most probably associated to both slipping and inter-laminar damage among the two embedded cables similar to quasi-static short 3 point bend tests, and to initiation of matrix cracking and delamination among the host composite structure as observed previously.

As predict in numerical model, transverse shear strains seem to initiate inter-laminar damage and delamination at the interface of the flat cable layers (Fig.15.a) and identify in the contact force histories (Fig. 15.b).
It is observed that the fibre tension-shear failure which seems to initiate at the interface with the embedded cables is a consequence of the sliding that occurs inside the embedded cables. Indeed, sliding among the cables first occurs and is well reproduced by the cohesive surface to-surface interaction. This triggers the first load drop observed experimentally at 0,8 ms. It induces higher inter-laminar and tensile strains on the adjacent composite plies, which leads to tension-shear fibre fracture captured at approximately 1,6ms

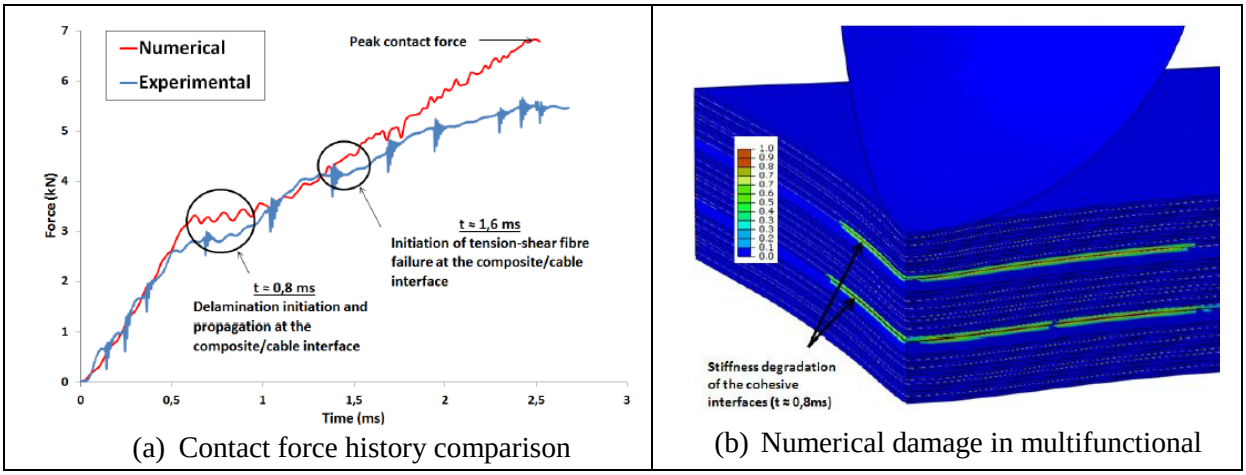

(a) Contact force history comparison (b) Numerical damage in multifunctional

Fig .15. Damage influence take into account by the numerical model

3.2. Post impact dielectric strength tests.

In order to study the influence of such damage mechanisms on the electrical functionality of the structure, post-impact dielectric strength tests were performed. In addition to the impact tests presented above, some additional test specimens were also impacted at 25J. Dielectric strength measurements are performed on electrical components to determine the effectiveness of their insulation [21, 22]. The basic principle is to apply an increasing voltage between two electrical conductors until dielectric breakdown of the material occurs. The higher the dielectric strength the better the quality of the insulation.
Reference dielectric strength tests were first performed on non-embedded cables with dielectric strength tester. No electrical shorting occurs between any conductors up to 10kV, which is the maximum capacity of the machine.

Post-impact dielectric strength tests were then performed on every impacted test specimens [23]. Different injection configurations were tested (between adjacent conductor on same layer and between superposed conductors), resulting in 13 dielectric strength tests per test specimens according to figure 16.b. (8 tests on adjacent conductors and 5 on superposed conductors).

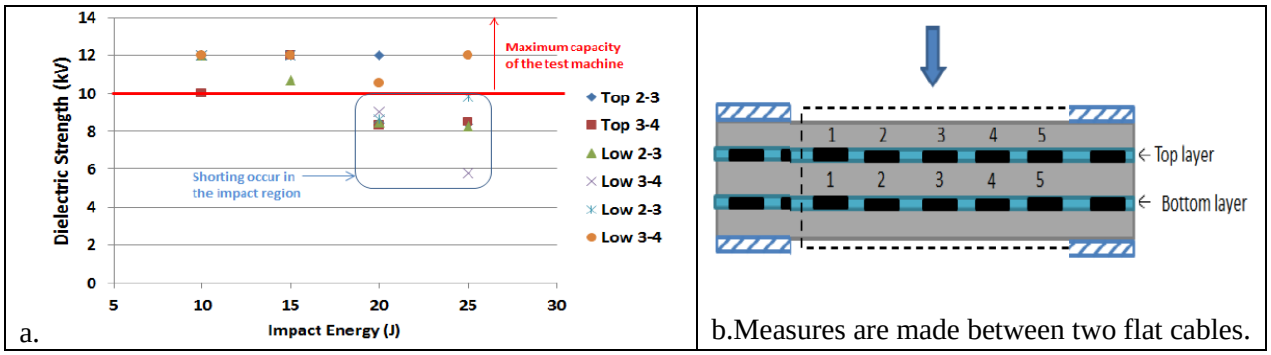

a. b.Measures are made between two flat cables.

Fig . 16. (a) Results of the post-impact dielectric strength tests, (b) configuration of the post impact dielectric strength.

These considerations led to the results presented in figure 16.a. where the dieletric strength (breakdown voltage in kV) is plotted versus the impact energy. So, no electrical shorting ever occurred on any test specimens impacted at 10J and 15J. For test specimens impacted at higher impact energies, electrical shorting did occur among the embedded cables (figure 16.a). It always occurred between two conductors of the same cable (adjacent conductors of the top or bottom cable).

Conclusion

Representative multifunctional composite structure specimens embedding two layers of flat cables are achieved for experimental quasi-static and dynamic test. Experimental tests aim for study the impact response of these structures and particularly influence of the embedded layers on failure.
The structure appeared to be particularly weakened when loaded in bending static and dynamic due to the low shear stiffness of the embedded cables which induced higher internal shear strains. Ultimately, these additional shear strains led to induced both internal fiber failure of composite plies at interface with embedded cables, and de-cohesions within the cables. In addition they may result in insulation degradation between adjacent wires, and alter electrical performances.
A progressive damage model coupled to cohesive elements is defined for correlation with test results. The model has the capability to get damage and failure mechanisms in accordance with experimental observation.
In addition, a methodology of characterization was developed to take the temperature-dependent stiffness through dynamic mechanical analyses into account [24].
This work help to define both design and electrical degradation criteria for the development of multifunctional sandwich architecture with embedding electrical cables for aeronautic specifications.

Acknowledgements

The authors would like to thank Mr Jesus ASPAS PUERTOLAS from ArianeGROUP, Les Mureaux, France, for this expertise in electromagnetic compatibility in aeronautical structures and the funding of the research.

References

[1] R. F. Gibson, ‘A review of recent research on mechanics of multifunctional composite materials and structures’, *Compos. Struct.*, vol. 92, no. 12, pp. 2793–2810, Nov. 2010.

[2] T. Vogel, ‘Multiphysics analyses and modelling for the development of composite structures embedding electrical wires’, thesis, 2017

[3] J.-K. Kim and M.-L. Sham, 'Impact and delamination failure of woven-fabric composites',*Compos. Sci. Technol.*, vol. 60, no. 5, pp. 745–761, 2000.

[4] A. S. Vaidya, U. K. Vaidya, and N. Uddin, 'Impact response of three-dimensional multifunctional sandwich composite', *Mater. Sci. Eng. A*, vol. 472, no. 1–2, pp. 52–58, Jan. 2008.

[5] F. Pinto, 'Smart Multifunctional Composite Materials for Improvement of Structural and non-structural properties', University of Bath, 2013.

[6] J.-C. Walrick, M. Grésil, and P. Parneix, 'Influence sur la tenue mécanique de l'insertion d'une fonction de protection électromagnétique au sein de composites à renforts de fibres de verre = Strength mechanical influence of electromagnetic shield function embedded in laminated glass composite', in *JNC 16*, 2009, p. 10

[7] M. Asaad, 'Damage accumulation in hybrid woven fabric composites', Bournemouth University, 2002

[8] O. T. Topac, 'Experimental and Numerical Investigation of Damage Process in Composite Laminates under Low-Velocity Impact', Middle East Technical University, 2016.

[9] 'AITM1-0010 - Airbus Test Method. Fiber Reinforced Plastics - Compression Strength After Impact', pp. 1–15, Oct-2005.

[10] J. R. Xiao, B. A. Gama, and J. W. Gillespie, 'Progressive damage and delamination in plain weave S-2 glass/SC-15 composites under quasi-static punch-shear loading', *Compos. Struct.*, vol. 78, no. 2, pp. 182–196, Apr. 2007.

[11] R. C. Batra, G. Gopinath, and J. Q. Zheng, 'Damage and failure in low energy impact of fiber-reinforced polymeric composite laminates', *Compos. Struct.*, vol. 94, no. 2, pp. 540–547, Jan. 2012.

[12] M. A. Hassan, S. Naderi, and A. R. Bushroa, 'Low-velocity impact damage of woven fabric composites: Finite element simulation and experimental verification', *Mater. Des.*, vol. 53, pp. 706–718, Jan. 2014.

[13] N. R. Mathivanan and J. Jerald, 'Experimental investigation of woven E-glass epoxy composite laminates subjected to low-velocity impact at different energy levels', *J. Miner. Mater. Charact. Eng.*, vol. 9, no. 07, p. 643, 2010.

[14] H. Ullah, A. R. Harland, and V. V. Silberschmidt, 'Dynamic bending behaviour of woven composites for sports products: Experiments and damage analysis', *Mater. Des.*, vol. 88, pp. 149–156, Dec. 2015.

[15] I. Ivañez, C. Santiuste, and S. Sanchez-Saez, 'FEM analysis of dynamic flexural behaviour of composite sandwich beams with foam core', *Compos. Struct.*, vol. 92, no. 9, pp. 2285–2291, Aug. 2010.

[16] H. Ullah, A. R. Harland, and V. V. Silberschmidt, 'Evolution and interaction of damage modes in fabric-reinforced composites under dynamic flexural loading', *Compos. Sci. Technol.*, vol. 92, pp. 55–63, Feb. 2014.

[17] 'MAT162 User's Manual Version 15A-2015', 2015.

[18] Z. Hashin, 'Failure criteria for unidirectional fibre composites', *Journal of Applied Mechanics*, pp. 329–334, 1980.

[19] A. Matzenmiller, J. Lubliner, and R. . Taylor, 'A constitutive model for anisotropic damage in fiber-composites', *Mechanics of Materials*, pp. 125–152, 1995.

[20] K. Song, C. G. Dávila, and C. A. Rose, 'Guidelines and parameter selection for the simulation of progressive delamination', 2008.

[21] 'NF-EN-ISO 3475: Aerospace series - Cables, Electrical, Aircraft use'.

[22] ESA, 'ESCC Detail Specification No. 3901/001, Polyimide insulated wires and cables, Low frequency, 600V, -100 to +200°C'. Issue 3, Jan-1996.

[23] T. Vogel, J.C. Walrick, P. Casari, 'Investigations on the damage of multifunctional structures under low energy impacts', JNC, 2017

[24] T. Vogel, M. Girard, P. Casari, J.C. Walrick, 'Investigations on the thermo-mechanical behaviour of a complex assembly through dynamic mechanical analyses', ICCS20, 2017